Binding, folding and insertion of a β-hairpin peptide at a lipid bilayer surface: Influence of electrostatics and lipid tail packing

Keon A. Reid, *Emory University*
Caitlin M. Davis, *Emory University*
Brian Dyer, *Emory University*
James Kindt, *Emory University*

Final published version: http://dx.doi.org/10.1016/j.bbamem.2017.12.019

Copyright information:

Binding, Folding and Insertion of a β-Hairpin Peptide at a Lipid Bi layer Surface: Influence of Electrostatics and Lipid Tail Packing

Keon A. Reid[1], **Caitlin M. Davis**[1,2], **R. Brian Dyer**[1], and **James T. Kindt**[1]

[1]Department of Chemistry, Emory University, 201 Dowman Drive, Atlanta, GA 30322

[2]Department of Chemistry and Department of Physics, University of Illinois at Urbana-Champaign, Urbana, Illinois, 61801

Abstract

Antimicrobial peptides (AMPs) act as host defenses against microbial pathogens. Here we investigate the interactions of SVS-1 (KVKVKVKV^{D}P^{L}PTKVKVKVK), an engineered AMP and anti-cancer β-hairpin peptide, with lipid bilayers using spectroscopic studies and atomistic molecular dynamics simulations. In agreement with literature reports, simulation and experiment show preferential binding of SVS-1 peptides to anionic over neutral bilayers. Fluorescence and circular dichroism studies of a Trp-substituted SVS-1 analog indicate, however, that it will bind to a zwitterionic DPPC bilayer under high-curvature conditions and folds into a hairpin. In bilayers formed from a 1:1 mixture of DPPC and anionic DPPG lipids, curvature and lipid fluidity are also observed to promote deeper insertion of the fluorescent peptide. Simulations using the CHARMM C36m force field offer complementary insight into timescales and mechanisms of folding and insertion. SVS-1 simulated at an anionic mixed POPC/POPG bilayer folded into a hairpin over a microsecond, the final stage in folding coinciding with the establishment of contact between the peptide's valine sidechains and the lipid tails through a "flip and dip" mechanism. Partial, transient folding and superficial bilayer contact are seen in simulation of the peptide at a zwitterionic POPC bilayer. Only when external surface tension is applied does the peptide establish lasting contact with the POPC bilayer. Our findings reveal the influence of disruption to lipid headgroup packing (via curvature or surface tension) on the pathway of binding and insertion, highlighting the collaborative effort of electrostatic and hydrophobic interactions on interaction of SVS-1 with lipid bilayers.
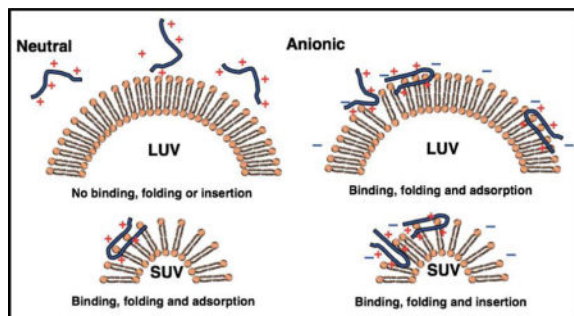
Graphical Abstract

1. Introduction

Antimicrobial peptides (AMP's) are short, charged membrane proteins that are ubiquitous in the tissues of plants, animals, and invertebrates and are typically comprised of 50 or fewer amino acids. They are amphiphiles composed of hydrophilic and hydrophobic amino acid residues adopting different structures (α-helical, β-stranded, β-hairpin, extended) [1,2]. In addition, they act as a host defense against microbial pathogens. AMPs display cytotoxic activity towards gram-positive and gram-negative bacteria, fungi and cancerous cells [3–10] and are selective towards negatively charged membranes, which allows AMPs to kill microorganisms without harming normal mammalian cells [5]. Cancer cells, in common with some bacteria, display a net negative charge on their surface [9]. Selectivity for disrupting anionic membranes therefore gives AMPs anticancer activity in addition to antimicrobial activity. However, the exact mechanisms by which AMPs disrupt these cells are still elusive.

Naturally occurring AMPs display a wide variety of sequences and structures. AMPs are generally disordered in solution, but fold into an ordered secondary structure when associated with lipid bilayers [11]. Several membrane disruption mechanisms have been proposed but none of them is applicable to all classes of AMPs [2,11,12]. The most prominent peptide-mediated membrane pore formation mechanisms are: the barrel stave pore, the carpet mechanism, the toroidal pore, the disordered toroidal pore, and electrostatic effects [1,2,11,13]. Factors such as peptide composition, secondary structure, peptide crowding and membrane composition all contribute to the overall function of AMPs in the presence of different biological membranes. High-resolution experimental techniques (such as NMR and X-ray crystallography) are unable to fully resolve AMP/lipid interactions and lytic mechanisms, thus computational techniques are needed to further molecular insight [2,14-16]. MD studies have been applied in this field to optimize the conformation of AMPs in the presence of membrane-mimicking solvent mixtures [1], to observe the adsorption process of the peptide into membrane mimics [10,14], and to study the spontaneous nature of peptide assembly that leads to membrane disruption [17–22] (For a thorough review of AMPs, please see references 6, 23-26).

Here we have investigated the bilayer interactions of SVS-1, a cationic AMP engineered to disrupt cancer cell membranes with low cytotoxicity towards noncancerous cells [5,25]. Specifically, spectroscopy studies and computer simulations examined the binding, folding and insertion of SVS-1 in the presence of zwitterionic or negatively charged lipid bilayers. According to Sinthuvanich et al. [5], SVS-1 is the first example of an anticancer β-hairpin whose action is dependent on membrane-induced folding. Lu et. al. also showed preferential folding of a hairpin in the presence of an anionic bilayer using NMR relaxation studies [27]. In the design of SVS-1, the unnatural D-enantiomer of proline (Pro) was used to create the β-turn in the secondary structure of the peptide sequence. The SVS-1 peptide (sequence KVKVKVKV^{D}P^{L}PTKVKVKVK) contains a D-Pro/L-Pro motif that folds into a structured Type II' β-turn [28] as shown in Figure 1 [5]. The alternating valine and lysine residues allow SVS-1 to adopt an amphiphilic structure, which is a common feature of AMPs and aids in aggregation and electrostatic interactions on the surface of anionic membranes. Though the peptide remains unfolded in solution or in the presence of zwitterionic membranes due to the positively charge lysine repulsions, the turn is structured because of the D-Pro and L-Pro isomers. SVS-1 is hypothesized to fold once it binds to a charged membrane due to complementary electrostatic interactions.

Consistent with past experiments, we found that SVS-1 does not bind to zwitterionic LUV in experiment or to stress-free zwitterionic bilayers in computer simulation. Interestingly, when curvature was introduced to the bilayer in experiments using zwitterionic small unilamellar vesicles (SUV), SVS-1 will bind to and fold at the surface of the membrane, based on CD and fluorescence experiments of a SVS-1 tryptophan analog. Similarly, in simulations SVS-1 was observed to fold and insert its valine sidechains into contact with the lipid tails of an anionic bilayer but to form few and transient contacts with an all-zwitterionic lipid bilayer. Only when the zwitterionic bilayer was placed under surface tension, increasing its area per lipid, did the peptide establish and maintain close contact with the bilayer. Together the results indicate that the fate of the peptide encountering the surface and inserting will depend on a combination of surface charge and solvent exposure of the hydrophobic tails.

2. Materials and Methods

2.1. Experimental Methods

2.1.1. Protein Synthesis and Purification—SVS-1 and tryptophan-substituted analog, SVS-V8W (KVKVKVKW^{D}P^{L}PTKVKVKVK), were synthesized via standard 9-fluorenylmethyloxycarbonyl (Fmoc) base solid-phase chemistry on a Liberty1 microwave peptide-synthesizer (CEM, Matthews, NC). Fmoc-PAL-PS resin (Applied Biosystems, Foster City, CA) was used to form a peptide amide. The peptide was purified by reverse-phase chromatography (C18 column) using a water/acetonitrile gradient with 0.1% trifluoroacetic acid (TFA) as the counter-ion. The peptide was lyophilized and dissolved in a 2 mM HCl solution to allow exchange of the TFA counter-ion for HCl [30]. The identity of the peptide was confirmed by matrix-assisted laser desorption ionization time-of-flight mass spectrometry. Stock peptide was prepared at 1 mM concentration in water.

2.1.2. Liposome Preparation—Lipids 1,2-dipalmitoyl-sn-glycero-3-phosphocholine (DPPC) and 1,2-dipalmitoyl-sn-glycero-3-phospho-(1′-rac-glycerol) (DPPG) and extrusion kit were purchased from Avanti Polar Lipids, Inc (Alabaster, Alabama). Large unilamellar vesicles (LUV) of 120-140 nm or small unilamellar vesicles (SUV) of 15-50 nm were used as a model system for fluorescence studies. Liposomes dissolved in chloroform were mixed at the desired molar ratio (1:1 PC/PG or pure PC) and dried by N_2 gas. Solvent removal was completed in a vacuum overnight. The lipid film was reconstituted in 20 mM sodium phosphate buffer and 300 mM NaCl pH 7.4. SUV were prepared by sonication above the transition temperature 41 °C. The suspension was sonicated until it changed from milky to clear in appearance. LUV were prepared by extrusion techniques. The lipid suspension was subjected to six freeze-thaw cycles and extruded using 100-nm pore size filters. Peptide and lipid were diluted to the desired molar ratio with a final buffer concentration of 10 mM sodium phosphate and 150 mM NaCl pH 7.4. The effective diameter of the vesicles was determined using dynamic light scattering (See Figure S1, Supporting Information).

2.1.3. CD Spectroscopy—CD wavelength scans were recorded on a Jasco J-810 spectropolarimeter equipped with a PFD-425S Jasco temperature controller module (Jasco, Inc., Easton, MD). All measurements were obtained using a 1-mm pathlength cell. Wavelength scans were recorded over the range of 260 to 200 nm with an average of 3 repeats. During spectral acquisition, a bandwidth of 2 nm and scan rate of 50 nm/min was used.

2.1.4. Fluorescence Spectroscopy—Fluorescence spectra were recorded on a HORIBA Dual-Fl Spectrofluorometer (HORIBA Scientific, Edison, NJ). All measurements were obtained using a 1.0 cm pathlength cuvette. The peptide was excited at 280 nm and monitored from 300 nm to 450 nm. Thermal experiments were monitored every 5 °C from 5 to 90 °C.

2.2. Simulation Methods

2.2.1. SVS-1 Structure—The SVS-1 hairpin structure was generated using the Molefacture Protein Builder tool of VMD (version 1.9) [29] and subject to energy minimization with constraints placed on the native hydrogen bonds. The peptide sequence was added into the Protein Builder to generate an unfolded SVS-1 structure, with an amidated –NH_2 C-terminus end used in experiment producing a +9 overall charge on the peptide. The phi/psi angles were selected to generate a Turn conformation for the folded peptide.

2.2.2. Bilayer Creation—The CHARMM-GUI membrane builder online software was used to generate a negatively charged POPC/POPG bilayer structure and a pure POPC bilayer [31-33]. The charged bilayer consists of 70 zwitterionic POPC (1-palmitoyl-2-oleoyl-sn-glycero-3-phosphocholine) lipids and 70 negatively charged POPG (1-palmitoyl-2-oleoyl-sn-glycero-3-phosphoglycerol). The pure POPC bilayer was composed of 140 lipids.

2.2.3. Molecular Dynamics Simulations—All simulations were performed using CHARMM 36m (C36m) [34] all-atom force field with the MD package Gromacs [35,36]. The simulation box size was subject to constant particle number, pressure, temperature (NPT) dynamics. Periodic boundary conditions were applied in the X and Y dimensions with semi-isotropic coupling using the Berendsen barostat [37] at 1 bar and a coupling constant of 1.0 ps. The compressibility factor used in both directions was 4.5×10^{-5} bar^{-1}. Simulations were conducted at 323 Kelvin (50 °C) using Velocity Rescaling [38]. TIPS3P waters [35], K^+ and Cl^- ions were added to neutralize the charge across the simulation box. Minimization to relax the structure of the system was conducted using the steepest descent method prior to conducting MD simulations. A MD integration timestep of 2 fs was used. VMD [29] was used to visualize trajectories and Gromacs analysis tools were utilized for reporting data. Simulations were carried out locally and via a XSEDE allocation [39].

We conducted 0.5-1.5 microsecond simulations with a single unfolded SVS-1 molecule in pure solution and in the presence of zwitterionic and charged bilayers (See Table 1). The peptide was initiated in solution approximately 2 nm from the surface of the zwitterionic or anionic lipid bilayer, starting with different peptide orientations. We probed the effects of stress by applying a surface tension to the bilayer in the X and Y dimensions. A series of simulations were conducted at 323 K and at applied surface tensions factors of 10 or 30 mN/m for 250 ns. Two types of trials were conducted for the negatively charged POPC/POPG bilayer where a pre-folded or unfolded SVS-1 peptide was placed in a random orientation approximately 1 nm above the membrane. Only pre-folded peptides were used for the POPC bilayer.

2.2.4. Data Analysis—Distance fluctuations were tracked between portions of the peptide and hydrophobic tails at long timescales. The terminal amine nitrogen (residue 1-LYS) and terminal carbonyl carbon (residue 18-LYS), along with the alpha carbon atom (residue 9-PRO) were selected to track the distance fluctuations to the nearest acyl tail carbon atom. Hydrogen bond formations were calculated for the eight correct backbone nitrogen donor and oxygen acceptor pairs of the peptide using Gromacs analysis tools. Cutoffs for hydrogen bond criterion are 3 Å and 20°. The valine contacts were tracked by counting the number of beta carbon valine CH side chain sites within 0.5 nm of any lipid acyl CH_2 or CH_3 tail site. Plots of H-bond and valine contacts are smoothed, showing averages over 1 ns. Area per lipid (APL) changes in bilayer was calculated by multiplying the X and Y box dimensions and dividing by 70, the number of lipids in a monolayer.

3. Results

3.1. Experimental Results

3.1.1. Concentration Dependence of Folding at Charged Surface—Folding of the SVS-1 peptide in 1:1 DPPC/DPPG LUV is highly dependent on the peptide:lipid ratio (Figure 2). Similar studies in DPPC LUV showed no significant changes in CD spectra under the same conditions, demonstrating the importance of electrostatics in SVS-1 binding and folding. Typically, β-sheet peptides have a CD spectrum with a negative peak at ~218 nm and a positive peak at ~195 nm [40]. Disordered peptides have low ellipticity above 210

nm and a negative band near 195 nm [41]. Above a peptide:lipid ratio of 1:12 the CD spectra is dominated by a negative peak at 198 nm, consistent with disordered structure. As the peptide:lipid ratio is decreased below 1:12 a negative peak at 218 nm and a positive peak at 200 nm appears, consistent with β-hairpin formation.

All experiments were carried out at a peptide:lipid ratio of 1:42, a ratio where SVS is folded in the presence of charged LUV and SUV (See Figure S2, Supporting Information). This ratio and the high melting DPPC:DPPG lipids were selected to minimize oligomerization. The first minimizes aggregation, which should be most prevalent at high peptide:lipid ratios where we observe the peptide to be disordered. The second minimizes insertion and membrane disruption at lower peptide:lipid ratios where the peptide folds at the charged membrane surface.

3.1.2. Curvature Induced Folding at Zwitterionic Membrane Surface—A tryptophan mutation was incorporated into SVS-1 as a fluorescent probe of the peptide insertion into the membrane. Valine 8 in the turn was selected as the mutation site for tryptophan, because both residues are hydrophobic and mutation of a residue in the sheet may disrupt the amphiphilic structure. We confirmed that the SVS-V8W mutant maintains selectivity for charged LUV by circular dichroism (See Figure S3, Supporting Information).

SVS-V8W and DPPC vesicles were used to test the role of curvature on β-hairpin folding at membrane surfaces. Far UV-CD was used to investigate the secondary structure of SVS-V8W in the presence and absence of model membranes, Figure 3. The CD spectra of SVS-V8W in buffer and in the presence of zwitterionic DPPC LUV exhibit a negative peak at ~198 nm and a positive peak at 223 nm. The negative peak at ~198 nm is consistent with the expected disordered structure. A positive peak at 220-230 nm arises from the presence of ordered aromatic side chains [40, 42]. A band at ~230 nm could also arise from exciton coupling between two tryptophans within 10 Å, for example if the peptide aggregated [43]. Such a scenario is unlikely, because the charged repulsion that restricts folding of the β-sheets would also deter aggregation. The SVS-1 peptide was designed with a type II' β-turn, V^DP^LPT, which is structured even in the absence of the β-sheets [5]. The small positive peak at 223 nm that lies on top of the large negative peak at ~198 nm (See Figure S4, Supporting Information) indicates that the tryptophan is in an ordered environment, likely packed within the structured turn. The β-sheets of the peptide are disordered leading to the random coil peak at ~198 nm. These experiments demonstrate that SVS-V8W is unfolded in solution and in the presence of zwitterionic LUV. However, the CD spectrum of SVS-V8W in the presence of zwitterionic DPPC SUV, which have a higher curvature, has a minimum at 218 nm and a maximum ~200 nm, consistent with β-sheet structure. This demonstrates that the peptide folds into a β-hairpin in the presence of lipids with high curvature. The absence of the 223 nm peak indicates that the tryptophan is no longer packed in the turn of the hairpin.

Fluorescence was used to investigate the environment of the tryptophan in the turn of SVS-V8W in the presence and absence of model membranes, Figure 4. Lipid-peptide interactions can be monitored through changes in the tryptophan fluorescence emission properties of the peptide upon interaction with the model membranes [44]. The fluorescence intensity and wavelength maximum of tryptophan are sensitive to its local environment and have been

correlated with the degree of solvent exposure of the chromophore [45–47]. A decrease in intensity and red shift of the maximum wavelength has been reported upon solvent exposure. The fluorescence spectra of SVS-V8W in buffer or DPPC LUV have similar overall intensity and maxima at ~347 nm (Figure 4). This supports the observation from the circular dichroism experiment that the structure of SVS-V8W is the same in buffer and in DPPC LUV. The slight difference in the DPPC LUV spectrum is due to light scattering of the excitation band in LUVs, which directly contributes to the observed emission signal at low wavelengths, decreases the overall observed intensity as less light reaches the tryptophans, and asymmetrically affects the tryptophan's excitation band resulting in a slight shift in maximum wavelength [48, 49]. In the presence of DPPC SUV the SVS-V8W fluorescence is slightly blue shifted to 342 nm, and has an overall increase in intensity. The tryptophan in SVS-V8W is less solvent exposed in the presence of DPPC SUV than in buffer or DPPC LUV. CD measurements showed that SVS-V8W is folded in DPPC SUV and that the tryptophan was not in a rigid environment, therefore solvent protection does not arise from the tryptophan packing into the β-hairpin. Instead, the increase in solvent protection suggests that SVS-V8W is folded at the surface of membranes with high curvature and that solvent protection of tryptophan arises from the tryptophan burying in the membrane. The tryptophan buried into the membrane surface is able to freely rotate, leading to the absence of the circular dichroism peak at ~230 nm (Figure 3). Interestingly, this implies that the SVS-V8W peptide does not associate with the LUV. If the peptide were at the surface of the LUV, the hydrophobic tryptophan would bury into the surface of the membrane, which provides greater solvent protection, and the CD peak at ~230 nm would disappear. This demonstrates the affinity of SVS-V8W for highly curved lipid surfaces.

3.1.3. Curvature Induced Insertion at Charged Surface—SVS-V8W and 1:1 DPPC/DPPG vesicles were used to test the role of curvature on β-hairpin folding and insertion at charged membrane surfaces. Far UV-CD confirmed that SVS-V8W is folded at the surface of both 1:1 DPPC/DPPG LUV and SUV (See Figure S5, Supporting Information). Fluorescence was used to investigate the environment of the tryptophan in the turn of SVS-V8W in the presence and absence of model membranes, Figure 5. The fluorescence spectra of SVS-V8W in 1:1 DPPC/DPPG LUV has a similar overall intensity and maxima at ~338 nm to SVS-V8W in DPPC SUV (Figure 4, Figure 5). Together with the absence of the ~230 nm peak in the CD spectra (Figure 2), this suggests that the tryptophan in 1:1 DPPC/DPPG LUV is buried in the vesicle similar to that in DPPC SUV. As expected from concentration dependent studies, the electrostatic interaction of SVS-V8W with 1:1 DPPC/DPPG LUV induces binding and folding of the β-hairpin. The fluorescence spectra of SVS-V8W in 1:1 DPPC/DPPG SUV is blue shifted from the 1:1 DPPC/DPPG LUV, 333 nm, and has an increase in intensity. The tryptophan is buried deeper in the SUV than the LUV. This demonstrates that SVS-V8W folding and insertion is sensitive to both electrostatic interactions and affinity for highly curved lipid surfaces.

3.1.4. Lipid Phase Induced Insertion at Charged Surface—Temperature-dependent experiments were conducted to study the dependence of the binding and insertion on the fluidity of the model membrane. One property of the vesicles is that the mobility of the individual lipid molecules changes with temperature from solid (gel) to liquid (fluid) phase.

As the temperature is raised the vesicle undergoes two transitions: a pre-transition from a gel phase to an intermediate "ripple" phase and main transition to the fluid phase. 1:1 DPPC/DPPG has a main phase transition temperature of 41 °C [50]. Fluorescence measurements of SVS-V8W in the presence of 1:1 DPPC/DPPG were taken every 5 °C over the course of a temperature scan from 5 to 65 °C (Figure 6 Inset). At low temperatures, the fluorescence intensity follows the typical temperature dependence due to the quantum yield of tryptophan [51]. As the melting temperature is approached there is an increase in intensity followed by a decrease. This transition was fit to an apparent two-state equilibrium model with a pre- and post-transition baseline to account for the temperature dependence of the tryptophan fluorophore on temperature:

$$A_0 = \frac{A_f + B_f T}{1 + exp\left(-\frac{\Delta H}{R}\left(\frac{1}{T} - \frac{1}{T_m}\right)\right)} + \frac{A_u + B_u T}{1 + exp\left(-\frac{\Delta H}{R}\left(\frac{1}{T} - \frac{1}{T_m}\right)\right)} \quad (1)$$

where A_0 is the observed absorbance, A_f and A_u are the absorbance contributions from the folded and unfolded populations, B_f and B_u are the baseline contributions from the temperature dependence of the tryptophan fluorophores in the folded and unfolded populations, ΔH is the enthalpy change at the midpoint, R is the gas constant, and T_m is the transition midpoint [52]. This transition fit with a T_m of 35 ± 1 °C, similar to the phase transition of 1:1 DPPC/DPPG LUVs, 41 °C. An increase in intensity near the phase transition of the LUV likely indicates further insertion of the peptide into the fluid phase. The increase in intensity is accompanied by a shift in the wavelength maximum; below the phase transition the maximum wavelength is 338 nm and above the phase transition the maximum wavelength is 333 nm (Figure 6). The data are normalized, because the strong temperature dependence of the tryptophan fluorophore makes it impossible to compare the relative intensity at the two temperatures. The wavelength of the maximum at high temperature in 1:1 DPPC/DPPG LUV is nearly identical to that in SUV (Figure 6). The fluorescence signal is broader in the LUV than SUV as there is more scattering from the larger vesicles. The peptide buries more deeply into the fluid phase of the vesicles than the gel phase, a behavior analogous to that observed for the AMP Mastoparan X [53]. This insertion process is irreversible; once the peptide has buried into the membrane at high temperature, there is no red shift or change in intensity as the membrane returns to the low-temperature phase (See Figure S6, Supporting Information). Together, these results suggests a model of binding, folding and insertion that is strongly driven by electrostatic interactions, but that can also be modulated by the peptide's affinity for highly curved surfaces and properties of the lipid components such as the phase transition.

3.2. Simulation Results

3.2.1. Characterizing folding and peptide-lipid interactions—Early steps of peptide-lipid interactions and peptide folding were modeled by all-atom MD simulations of the peptide in solution and in the presence of zwitterionic or anionic lipid bilayers. In a 1 μs simulation of the peptide in solution using the C36m force field, dynamic folding and unfolding are observed (Figure 7) and 1–2 of the native hairpin hydrogen bonds are formed on average. These hydrogen bonds are found close to the peptide turn where the hairpin

structure is strongly influenced by the ^{D}Pro-^{L}Pro motif [5,54]. Figure 7 shows snapshots of the different folded and extended states witnessed in solution. We note that simulations using the original C36 force field showed significant alpha-helical content in the solution-phase peptide conformation; for more discussion, please see Supplemental Information Section 4, Table S1, Figure S7.

Simulations of SVS-1 interaction with lipid bilayers were conducted on a pure zwitterionic POPC bilayer and a 1:1 POPC/POPG mixture. By using the anionic POPG lipid with one monounsaturated tail, we mimic the PG headgroups of the saturated DPPG lipids used in our experiments, avoid complications arising from unpredictable phase behavior in the simulation model encountered using saturated lipid tails, (See Figure S8, Supplemental Information), and eliminate the possibility of hydrogen bonding with serine POPS headgroups [59] used in earlier [5] experiments.

Simulations modeled the initial stage of contact of the unfolded peptide with the bilayer. During a 500 ns trajectory, SVS-1 makes only transient contact with the POPC bilayer via its N-terminus (Figure 8, upper left panel). Its folding behavior is similar to that seen in solution, switching between completely unfolded and partially folded states (Figure 8, lower left panel). In contrast, an initially unfolded SVS-1 interacting with the anionic POPC/POPG mixed bilayer maintains close contact with the bilayer (through its N-terminus or turn region) throughout a 1.5 μs simulation (Figure 8, upper right panel). Four pairs of H-bonding sites approach each other within the first 100 ns of contact (Figure 8, lower right panel) and the peptide maintains a partially folded structure with 3 to 5 bonds in contact, for over 1 microsecond. The partially folded structure presents the lysine side-chains towards the charged lipid headgroups, leaving the hydrophobic valine side-chains facing the solvent (Figure 9A).

Simulation reveals a novel insertion mechanism we coin the "flip and dip" mechanism. After a microsecond, the ^{D}Pro-^{L}Pro turn region dips into the bilayer interior (1075 ns, Figure 9B) while at the same time the hairpin twists (1080-1110 ns, Figure 9C) and brings the Val sidechains into contact with the bilayer interior (Figure 8, upper right). As the turn buries, the N-terminus (black curve) which had stayed close to the surface pops off while the C-terminus (red curve) moves in towards the lipid tails. Finally, the N-terminus joins the turn and the C-terminus in contact with the lipid tails, while the sixth and seventh pairs of hydrogen bonding sites along the hairpin come into close contact, effectively completing the folding process (Figure 8, lower right). A jump in the counts of valine side-chain contacts with the lipid tails to an average near 7 confirms that the peptide has made full hydrophobic contact (See Figure S9, Supplemental Information). Once buried beneath the headgroups, the peptide retains a high degree of folding until the end of the simulation (Figure 9D). Interactions between most Lys sidechains and bilayer headgroups can be maintained as the sidechains rotate around from pointing inward toward the bilayer to pointing outward toward the solvent (See Movie S1, Supplemental Information). In previously reported coarse-grained simulations [56], the valine sidechains folded under the headgroups from a similar on-top, valine-out state within about 50 ns. This mechanism is much slower within the atomistic model due to the greater constraints on backbone dihedrals.

3.2.2. Effects of Surface Tension on SVS-1 Insertion—To facilitate interaction of the valine sidechains with lipid tails, we perform simulations under applied surface tension. Increasing surface tension on the bilayer increases the bilayer surface area per lipid, exposing more of the hydrophobic interior to the solvent and the adsorbed peptide. This added exposure may be present in the highly curved external leaflets of SUVs [57], in fluid domains embedded in gel phase near T_m [58], in domain boundaries in SUV's below the bulk transition temperature [59], or under crowded conditions in which lateral pressure among surface adsorbates leads to expansion of the underlying membrane [60].

Simulations of modest length (250 ns) were performed under varying degrees of surface tension with either zwitterionic (POPC) or anionic (POPC/POPG) lipid bilayers and with the peptide either initiated in a folded or an unfolded state. As mentioned above, an ideal fully-folded SVS-1 hairpin structure contains eight characteristic hydrogen bonds; we never see the eighth h-bond formed consistently. Taking into account fluctuations across the H-bond cut-off criteria, we consider averaged hydrogen bond content of 3-4 to be partially folded and five or above to be fully folded. The N-terminal arm contains 4 valines while the C-terminal arm contains 3, so structures with 2-4 valines in contact with lipid tails likely have one arm embedded in the bilayer while contact by 5 or more valines indicates that both arms are embedded.

A pre-folded peptide was introduced to a zwitterionic membrane experiencing surface tensions of 10 mN/m and 30 mN/m, whereas both an unfolded and a pre-folded peptide were placed in the presence of the anionic membrane under the same conditions. Figure 10 depicts the valine contacts and hydrogen bond formation for results. In each folded peptide trajectory, the plots show 3-4 hydrogen bonds formed at the earliest timepoint plotted because the peptide partially unfolded within the first nanosecond, in solution or during initial contact with the bilayer. Interactions of the peptide with the surfaces under 10 mN/m surface tension were qualitatively similar from those seen in the longer trajectories in the absence of surface tension, with somewhat increased levels of hydrophobic contact; the peptide unfolded and made only sporadic contact with POPC, and maintained partial folding and partial hydrophobic contact with the POPG/POPC surface over 250 ns.

Increase of the surface tension to 30 mN/m changes the interactions between the peptide and bilayer significantly. In the case of SVS-1 interacting with POPC, by 75 ns the peptide has made full hydrophobic contact with the bilayer interior, inserting via the turn by a pathway similar to that seen in the 1.5 μs tension-free POPG/POPC simulation, and remains in strong hydrophobic contact for the remainder of the trajectory. The degree of folding increases somewhat during or directly after this insertion, but the peptide then gradually loses its folded structure. The anionic surface under 30 mN/m tension promotes rapid insertion of the initially unfolded peptide, apparently preventing or slowing further folding.

We note that the peptide's behavior observed in any of these single trajectories is just a sample of multiple possible outcomes that would appear in repeated trajectories with different initial orientations, etc., but nonetheless can see some trends from the simulations in the presence and absence of applied tension. In these simulations, SVS-1 peptides do not stick to the zwitterionic POPC surface unless hydrophobic contact is made; without exposed

hydrophobic surface (which we produce using applied surface tension, but whose presence might be expected for highly curved small unilamellar vesicles) desorption is rapid. At the PC/PG surface, electrostatics bind the peptide to the bilayer, so that initially unfolded SVS-1 can either begin to fold atop the bilayer surface before making full hydrophobic contact with the lipid tails (as seen in the absence of surface tension or at 10 mN/m) or, when the bilayer's hydrophobic interior is exposed under high surface stress, can rapidly engage in hydrophobic contact with the bilayer without folding.

4. Discussion

The new experimental data add to the known understanding of SVS-1 hairpin interactions with membranes by providing evidence for binding (under particular phase and curvature conditions) to zwitterionic bilayers and for differences in the depth of insertion under varying conditions. The simulation results offer some insight into timescales and mechanisms of folding and insertion, and possible structures of the bilayer-associated peptide.

The experimental concentration dependence data for charged DPPC/DPPG mixture suggests a range of 40–60 lipids/peptide is needed for optimum binding, suggesting an area requirement of ~15 nm^2 or a requirement for about 12 negative charges on the outer leaflet to compensate the 9 positive charges on the peptide (note that this is for large vesicles and at 20 °C, well below T_m). The most unexpected experimental observation, given previous reports of the inability of SVS-1 to bind to or fold in the presence of zwitterionic bilayer surfaces, is that the SVS-V8W folds in the presence of small DPPC vesicles (but not large ones) at temperatures below T_m. The size dependence suggests that curvature plays an important role. Details of the differences between large and small vesicles, especially under temperature conditions where a flat bilayer would be in the ordered, relatively rigid gel phase, are not entirely clear. It is likely, based on electron microscopy [61,62] and simulations of simple models [63–67] that the curvature needed for a closed structure is not spread evenly throughout the surface but is concentrated at disordered ridges that connect flat ordered facets. Relative to an LUV, an SUV will have a greater proportion of its surface occupied by ridge defects and is likely to have a greater localized curvature, which typically will produce a greater spacing between headgroups on the outer leaflet and more exposure of the hydrophobic tails [57].

Simulations of SVS-1 interaction with charged and zwitterionic lipid surfaces in the fluid phase are broadly consistent with the observed experimental behavior and suggest a pathway for preliminary stages in surface binding and folding. Unfolded SVS-1 interacts only transiently and superficially with the POPC surface but binds tightly to the POPC/POPG surface. In the latter case, folding was seen to proceed gradually over 100's of nanoseconds with the peptide's cationic lysine side-chains largely facing towards the lipid head-groups and most of the hydrophobic valine side-chains facing the solvent. Full contact between the hydrophobic valine side-chains and the lipid tails was made upon a "flip and dip" transition, which coincided with a jump in the degree of folding. The "flip and dip" mechanism of the on-top folded state, a cascading rotation of the peptide backbone promoted by valine insertion, can be contrasted with the rapid insertion seen in CG simulation under tension-

free conditions [56], where the side chains can just invert due to much lower torsional barriers.

Simulations of SVS-1 showed that it can bind to a POPC surface that is significantly expanded in its area per headgroup through application of 30 mN/m surface tension, and follow a similar "flip and dip" transition marked by a (transient) jump in the degree of folding. It seems that the zwitterionic surface under tension is able to stabilize the hairpin temporarily, in the absence of the electrostatic screening provided by the anionic headgroups, by providing an environment favorable to the amphiphilic arrangement of Lys and Val side-chains in the folded state. In contrast to the hairpin state of SVS-1 and SVS-V8W bound to SUV's of DPPC evident from CD spectroscopy, the SVS-1 peptide unfolded after insertion of its valine sidechains into the POPC bilayer under tension. It may be that the binding environment of an SUV below its transition temperature, which is likely characterized by small disordered domains interspersed among ordered domains that are presumed inaccessible to the peptide, constraints of the domain size or from other adsorbed peptides might stabilize the more compact, folded state.

In addition to facilitating the binding and folding of SVS-1 at the DPPC surface, curvature appears to influence the nature of binding of SVS-V8W at the DPPC/DPPG surface. The greater shift in Trp fluorescence shows a deeper binding state for the peptide bound to SUV than to LUV, at low temperatures. Interestingly, the peptide bound to low-temperature LUV will change irreversibly to a deeper binding state upon raising the temperature above T_m. The irreversible nature of this change is evidence that a qualitatively different structure, separated by an activation barrier, is at play as opposed to a difference in degrees of submergence. The less-deep state is also characteristic of the bound state of the zwitterionic DPPC LUV. We suggest that this is a shallow, folded subsurface state, similar to what we observe in simulations with the POPC/POPG bilayer (e.g. Figure 9d) or forming at a DPPC/DPPG bilayer surface in a ripple phase environment in simulation (See Figure S8, Supplemental Information). Formation of the deeper state, presumably a lytically active state that we have not seen in simulations, thus appears to require a combination of charged headgroups and a sufficiently fluid lipid environment. These requirements suggest that the headgroups may be an integral part of the deeply inserted state, perhaps as part of a toroidal structure with the headgroup charges interacting with the lysine sidechains. This would contrast with the beta-barrel structures modeled by Gupta et al. [12] in a study of the closely related MAX1 peptide, structures which do not provide for interactions between the anionic headgroups and the lysines in the peptide pore. In fact, some instability of the simulated beta-barrel structures in that study was attributed to Lys-Lys repulsions. In a toroidal structure, these repulsions would be screened by the anionic headgroups, albeit at the cost of disrupting intermolecular hydrogen bonds between peptide backbones. The relative stabilities of these different structures (or perhaps some intermediate state, with the beta-barrel only disrupted at one or more locations) could be a topic for future simulation studies.

5. Conclusions

Using circular dichroism and fluorescence spectroscopy it is possible to monitor differences in the fold and environment of the SVS-1 hairpin or its SVS-V8W analog. Similar to

previous experiments we observe that the peptide is unfolded in solution or in the presence of zwitterionic LUVs, but folds in the presence of charged LUVs. Interestingly, we observe that this process depends on curvature. In zwitterionic SUVs the peptide folds, while the peptide inserts deeper into charged SUVs than charged LUVs. Insertion is also shown to be dependent on the phase of the LUVs, with the peptide inserting further into the fluid phase vesicles.

Simulation results suggest that SVS-1 binds strongly to anionic lipids at the surface, adopting an initial configuration with its valine sidechains facing away from the bilayer surface. (SVS-1 associates only transiently with the surface of the zwitterionic POPC membrane, unless sufficient surface tension is applied to produce enhanced binding and insertion through hydrophobic exposure.) At the charged bilayer surface, SVS-1 gradually and reversibly adopts a hairpin structure over 100's of nanoseconds, with most of its valines remaining far from the hydrophobic lipid tails. A transition to a state with significant contact between the hydrophobic face of the peptide and the lipid tails was observed to involve an initial dip of the ^{D}Pro-^{L}Pro turn accompanied by a flip of the valine side-chains beneath the lipid head-groups. We have no simulation evidence for pore-like structures, which probably require cooperative behavior of multiple peptides. We speculate, however, that the different degrees of insertion (inferred from fluorescence spectra of SVS-V8W) observed depending on temperature and lipid charge may reflect the presence or absence of toroidal pores, whose stability would be influenced by the bilayer's flexibility and ability to screen the electrostatic repulsions among embedded peptides.

Supplementary Material

Refer to Web version on PubMed Central for supplementary material.

Acknowledgments

Abbreviations

| AMPs	antimicrobial peptides
ACPs	anticancer peptides
SUVs	small unilamellar vesicles
LUVs	large unilamellar vesicles
MD	Molecular Dynamics simulation
CD	circular dichroism

References

1. Yeaman MR, Yount NY. Mechanisms of antimicrobial peptide action and resistance. Pharmacological Reviews. 2003; 55(1):27–55. [PubMed: 12615953]

2. Bond PJ, Khalid S. Antimicrobial and Cell-Penetrating Peptides: Structure, Assembly and Mechanisms of Membrane Lysis via Atomistic and Coarse-Grained Molecular Dynamic Simulations. Protein and Peptide Letters. 2010; 17(11):1313–1327. [PubMed: 20673230]

3. Nakatsuji T, Gallo RL. Antimicrobial Peptides: Old Molecules with New Ideas. J Invest Dermatol. 2012; 132(3):887–898. [PubMed: 22158560]

4. Giuliani A, Pirri G, Nicoletto S. Antimicrobial peptides: an overview of a promising class of therapeutics. Cent Eur J Biol. 2007; 2(1):1–33.

5. Sinthuvanich C, Veiga AS, Gupta K, Gaspar D, Blumenthal R, Schneider JP. Anticancer β-Hairpin Peptides: Membrane-Induced Folding Triggers Activity. JACS. 2012; 134(14):6210–6217.

6. Fjel CD, Hiss JA, Hancock REW, Schneider G. Designing antimicrobial peptides: form follows function. Nat Rev Drug Discov. 2012; 11:37–51.

7. Brown KL, Hancock RE. Cationic host defense (antimicrobial) peptides. Curr Opin Immunol. 2006; 18(1):24–30. [PubMed: 16337365]

8. Zhao J, Zhao C, Liang G, Zhang M, Zheng J. Engineering Antimicrobial Peptides with Improved Antimicrobial and Hemolytic Activities. J Chem Inf Model. 2013; 53:3280–3296. [PubMed: 24279498]

9. Hoskin DW, Ramamoorthy A. Studies on anticancer activities of antimicrobial peptides. BBA Biomembranes. 2008; 1778(2):357–375. [PubMed: 18078805]

10. Gaspar D, Veiga AS, Castanho MARB. From antimicrobial to anticancer peptides. A review. Frontiers in Microbiology. 2013; 4:1–16. [PubMed: 23346082]

11. Shai Y, Makovitzky A, Avrahami D. Host defense peptides and lipopeptides: modes of action and potential candidates for the treatment of bacterial and fungal infections. Curr Protein Pept Sci. 2006; 7:479–486. [PubMed: 17168781]

12. Gupta K, Jang H, Harlen K, Puri A, Nussinov R, Schneider JP, Blumenthal R. Mechanism of membrane permeation induced by synthetic β-hairpin peptides. Biophysical Journal. 2013; 105(9): 2093–2103. [PubMed: 24209854]

13. Jean-François F, Elezgaray J, Berson P, Vacher P, Dufourc EJ. Pore Formation Induced by an Antimicrobial Peptide: Electrostatic Effects. Biophysical Journal. 2008; 95(12):5748–5756. [PubMed: 18820233]

14. Langham A, Kaznessis YN. Molecular Simulations of Antimicrobial Peptides. Methods in Molecular Biology. 2010; 618:267–285. [PubMed: 20094870]

15. Nguyen LT, Haney EF, Vogel HJ. The expanding scope of antimicrobial peptide structures and their modes of action. Trends in Biotechnology. 2012; 29(9):464–470.

16. Harris F, Dennison SR, Singh J, Phoenix DA. On the selectivity and efficacy of defense peptides with respect to cancer cells. Medicinal Research Reviews. 2013; 33(1):190–234. [PubMed: 21922503]

17. Shai Y. Mode of action of membrane active antimicrobial peptides. Biopolymers. 2002; 66:236–248. [PubMed: 12491537]

18. Leontiadou H, Mark AE, Marrink SJ. Antimicrobial Peptides in Action. JACS. 2006; 128:12156–12161.

19. Biggin PC, Bond PJ. Molecular dynamics simulations of membrane proteins. Methods Mol Biol. 2008; 443:147–60. [PubMed: 18446286]

20. Biggin PC, Sansom MS. Interactions of alpha-helices with lipid bilayers: a review of simulation studies. Biophys Chem. 1999; 76(3):161–83. [PubMed: 10074693]

21. Gumbart J, Wang Y, Asksimentiev A, Tajkhorshid E, Schulten K. Molecular dynamics simulations of proteins in lipid bilayers. Curr Opin Struct Biol. 2005; 15:423–431. [PubMed: 16043343]

22. Matyus E, Kandt C, Tieleman DP. Computer simulation of antimicrobial peptides. Curr Med Chem. 2007; 14(26):2789–98. [PubMed: 18045125]

23. Zhao JZC, Liang G, Zhang M, Zheng J. Engineering Antimicrobial Peptides with Improved Antimicrobial and Hemolytic Activities. J Chem Inf Model. 2013; 53:3280–3296. [PubMed: 24279498]

24. Teixeira V, Feio MJ, Bastos M. Role of lipids in the interaction of antimicrobial peptides with membranes. Progress in Lipid Research. 2012; 51(2):149–177. [PubMed: 22245454]

25. Freire JM, Gaspar D, Veiga AS, Castanho MARB. Shifting gear in antimicrobial and anticancer peptides biophysical studies: from vesicles to cells. Journal of Peptide Science. 2015; 21(3):178–185. [PubMed: 25645747]

26. Gabernet G, Muller AT, Hiss JA, Schneider G. Membranolytic anticancer peptides. MedChemComm. 2016; 7(12):2232–2245.

27. Lu J-X, Damodaran K, Blazyk J, Lorigan GA. Solid-State Nuclear Magnetic Resonance Relaxation Studies of the Interaction Mechanism of Antimicrobial Peptides with Phospholipid Bilayer Membranes. Biochemistry. 2005; 44(30):10208–10217. [PubMed: 16042398]

28. Nair CM, Vijayan M, Venkatachalapathi YV, Balaram PJ. X-ray crystal structure of pivaloyl-D-pro-L-pro-L-ala-N-methylamide; observation of a consecutive β-turn conformation. J Chem Soc Chem Commun. 1979; 24:1183–1184.

29. Humphrey W, Dalke A, Schulten K. VMD: visual molecular dynamics. J Mol Graph. 1996; 14(33–38):27–28.

30. Andrushchenko VV, Vogel HJ, Prenner E. J Optimization of the hydrochloric acid concentration used for trifluoroacetate removal from synthetic peptides. Journal of Peptide Science. 2007; 13:37–43. [PubMed: 17031869]

31. Jo S, Kim T, Iyer VG, Im W. CHARMM-GUI: A Web-based Graphical User Interface for CHARMM. J Comput Chem. 2008; 29:1859–1865. [PubMed: 18351591]

32. Wu EL, et al. CHARMM-GUI Membrane Builder Toward Realistic Biological Membrane Simulations. J Comput Chem. 2014; 35:1997–2004. [PubMed: 25130509]

33. Brooks BR, et al. CHARMM: The Biomolecular Simulation Program. J Comput Chem. 2009; 30:1545–1614. [PubMed: 19444816]

34. Huang J, Rauscher S, Nawrocki G, Ran T, Feig M, de Groot BL, Grubmuller H, MacKerell AD Jr. CHARMM36m: an improved force field for folded and intrinsically disordered proteins. Nat Meth. 2017; 14(1):71–73.

35. Bjelkmar P, Larsson P, Cuendet MA, Hess B, Lindahl E. Implementation of the Charmm Force Field in Gromacs: Analysis of Protein Stability Effects from Correction Maps, Virtual Interaction Sites, and Water Models. J Chem Theory Comput. 2010; 6:459–466. [PubMed: 26617301]

36. Abraham MJ, Murtola T, Schulz R, Páll S, Smith JC, Hess B, Lindahl E. GROMACS: High performance molecular simulations through multi-level parallelism from laptops to supercomputers. SoftwareX. 2015; 1–2:19–25.

37. Berendsen HJC, et al. J Chem Phys. 1984; 81:3684–90.

38. Bussi G, Davide D, Michele P. Canonical sampling through velocity rescaling. J Chem Phys. 2007; 126(1):014101. [PubMed: 17212484]

39. Towns J, et al. XSEDE: Accelerating Scientific Discovery. Computing in Science & Engineering. 2014; 16(5):62–74.

40. Manning MC, Woody R. W Theoretical Determination of the Cd of Proteins Containing Closely Packed Antiparallel Beta-Sheets. Biopolymers. 1987; 26:1731–1752. [PubMed: 3663854]

41. Venyaminov S, Baikalov IA, Shen ZM, Wu CS, Yang J. T Circular dichroic analysis of denatured proteins: inclusion of denatured proteins in the reference set. Analytical Biochemistry. 1993; 214:17–24. [PubMed: 8250221]

42. Woody RW. Contributions of tryptophan side chains to the far-ultraviolet circular dichroism of proteins. Eur Biophys J. 1994; 23:253–262. [PubMed: 7805627]

43. Gasymov OK, Abduragimov AR, Glasgow BJ. Double tryptophan exciton probe to gauge proximal side chains in proteins: augmentation at low temperatur. J Phys Chem B. 2015; 119:3962–3968. [PubMed: 25693116]

44. Christiaens B, Symoens S, Vanderheyden S, Engelborghs Y, Joliot A, Prochiantz A, Vandekerckhove J, Rosseneu M, Vanloo B. Tryptophan fluorescence study of the interaction of penetratin peptides with model membranes. Eur J Biochem. 2012; 269:2918–2926.

45. Beechem JM, Brand L. Time-Resolved Fluorescence of Proteins. Annual Review of Biochemistry. 1985; 54:43–71.

46. Weber G. Fluorescence-Polarization Spectrum and Electronic-Energy Transfer in Tyrosine, Tryptophan and Related Compounds. Biochem J. 1960; 75:335–345. [PubMed: 13843297]

47. Eftink MR. Fluorescence Techniques for Studying Protein-Structure. Methods Biochem Anal. 1991; 35:127–205. [PubMed: 2002770]

48. Ladokhin AS, Jayasinghe S, White SH. How to measure and analyze tryptophan fluorescence in membranes properly, and why bother. Anal Biochem. 2000; 285:235–245. [PubMed: 11017708]

49. Moon CP, Fleming KG. Using tryptophan fluorescence to measure the stability of membrane proteins folded in liposomes. Methods Enzymol. 2011; 492:189–211. [PubMed: 21333792]

50. Silvius, JR. Lipid-Protein Interactions. John Wiley & Sons; New York: 1982. Thermotropic Phase Transitions of Pure Lipids in Model Membranes and their Modifications by Membrane Proteins.

51. Kirby EP, Steiner RF. Influence of solvent and temperature upon the fluorescence of indole derivatives. J Chem Phys. 1970; 74:4480–4490.

52. Nicholson EM, Scholtz JM. Conformational stability of the Escherichia coli HPr protein: Test of the linear extrapolation method and a thermodynamic characterization of cold denaturation. Biochemistry. 1996; 35:11369–11378. [PubMed: 8784192]

53. Schuler EE, Nagarajan S, Dyer RB. Submillisecond Dynamics of Mastoparan X Insertion into Lipid Membranes. J Phys Chem Lett. 2016; 7:3365–3370. [PubMed: 27513014]

54. Gaspar D, Veiga AS, Sinthuvanich C, Schneider JP, Castanho MARB. Anticancer Peptide SVS-1: Efficacy Precedes Membrane Neutralization. Biochemistry. 2012; 51(32):6263–6265. [PubMed: 22839778]

55. Jurkiewicz P, Cwiklik L, Vojtíšková A, Jungwirth P, Hof M. Structure, dynamics, and hydration of POPC/POPS bilayers suspended in NaCl, KCl, and CsCl solutions. BBA Biomembranes. 2012; 1818(3):609–616. [PubMed: 22155683]

56. Ganesan SJ, Xu H, Matysiak S. Effect of lipid head group interactions on membrane properties and membrane-induced cationic beta-hairpin folding. Phys Chem Chem Phys. 2016; 18(27):17836–17850. [PubMed: 27165814]

57. Cui H, Lyman E, Voth GA. Mechanism of Membrane Curvature Sensing by Amphipathic Helix Containing Proteins. Biophys J. 2011; 100(5):1271–1279. [PubMed: 21354400]

58. Yang L, Kindt JT. Line Tension Assists Membrane Permeation at the Transition Temperature in Mixed-Phase Lipid Bilayers. J Phys Chem B. 2016; 120(45):11740–11750. [PubMed: 27780354]

59. Patel LA, Kindt JT. Coarse-grained molecular simulations of the melting kinetics of small unilamellar vesicles. Soft Matter. 2016; 12(6):1765–1777. [PubMed: 26701014]

60. Busch DJ, Houser JR, Hayden CC, Sherman MB, Lafer EM, Stachowiak JC. Intrinsically disordered proteins drive membrane curvature. Nat Commun. 2015; 6

61. Andersson M, Hammarstroem L, Edwards K. Effect of Bilayer Phase Transitions on Vesicle Structure, and its Influence on the Kinetics of Viologen Reduction. J Phys Chem. 1995; 99(39):14531–14538.

62. Ickenstein LM, Arfvidsson MC, Needham D, Mayer LD, Edwards K. Disc formation in cholesterol-free liposomes during phase transition. BBA Biomembranes. 2003; 1614(2):135–138. [PubMed: 12896806]

63. Spangler EJ, Sunil Kumar PB, Laradji M. Anomalous freezing behavior of nanoscale liposomes. Soft Matter. 2012; 8(42):10896–10904.

64. Wu H-L, Sheng Y-J, Tsao H-K. Phase behaviors and membrane properties of model liposomes: Temperature effect. J Chem Phys. 2014; 141(12):124906. [PubMed: 25273473]

65. Risselada HJ, Marrink SJ. The freezing process of small lipid vesicles at molecular resolution. Soft Matter. 2009; 5(22):4531–4541.

66. Sknepnek R, Vernizzi G, Olvera de la Cruz M. Buckling of multicomponent elastic shells with line tension. Soft Matter. 2012; 8(3):636–644.

67. Bowick MJ, Sknepnek R. Pathways to faceting of vesicles. Soft Matter. 2013; 9(34):8088–8095.

Paper Highlights

- Electrostatic and hydrophobic interactions regulate binding, folding and insertion of SVS-1.

- Charged membranes promote and stabilize folding at the surface.

- Binding and folding observed at surface of small vesicles, but not large vesicles, of zwitterionic lipids.

- Simulations show a "flip and dip" mechanism of partial insertion of the peptide into the bilayer.
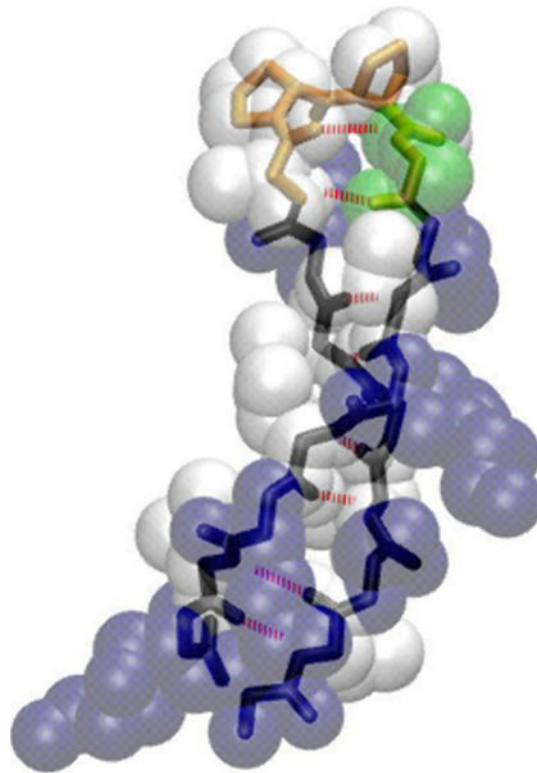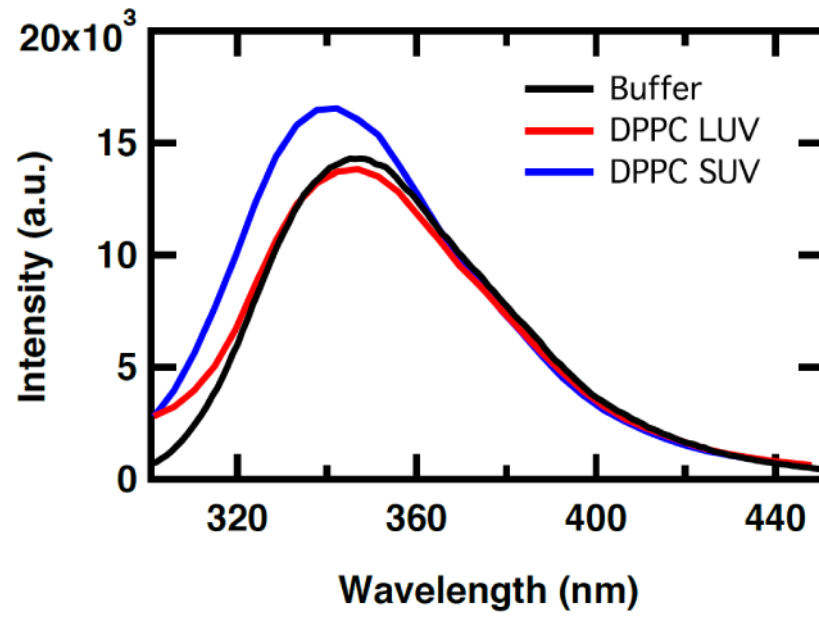
Figure 1.
Model of folded SVS-1 structure created using Visual Molecular Dynamics (VMD) [29].
Peptide backbone (black) is represented as a licorice, and V^{D}P^{L}PT turn motif colored in
orange. Peptide sidechains are presented as VDW beads – hydrophobic valines and prolines
(white), basic lysine (blue) and polar threonine (green). The intermolecular backbone
hydrogen bonds are drawn in red.
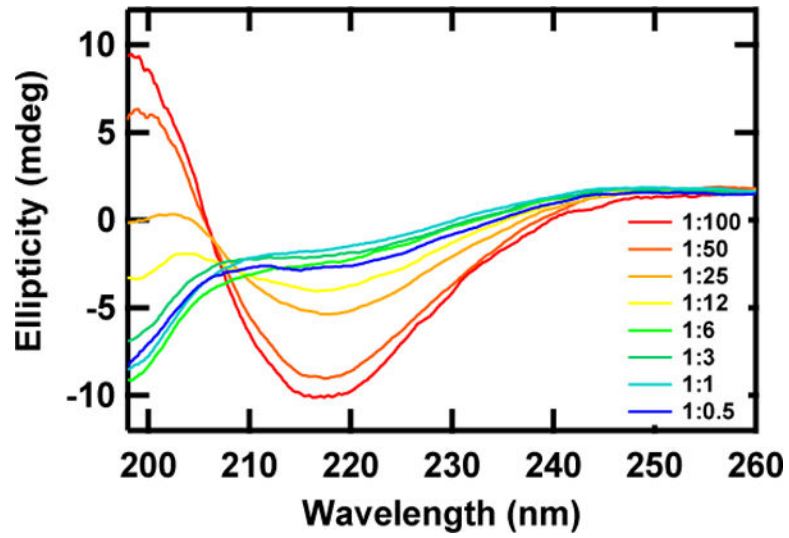
Figure 2.
Far-UV CD spectra of 50 μM SVS-1 mixed with 1:1 DPPC/DPPG LUV at molar ratios between 1:100 and 1:0.5 in 10 mM sodium phosphate buffer, 150 mM NaCl pH 7.4 at 20 °C.
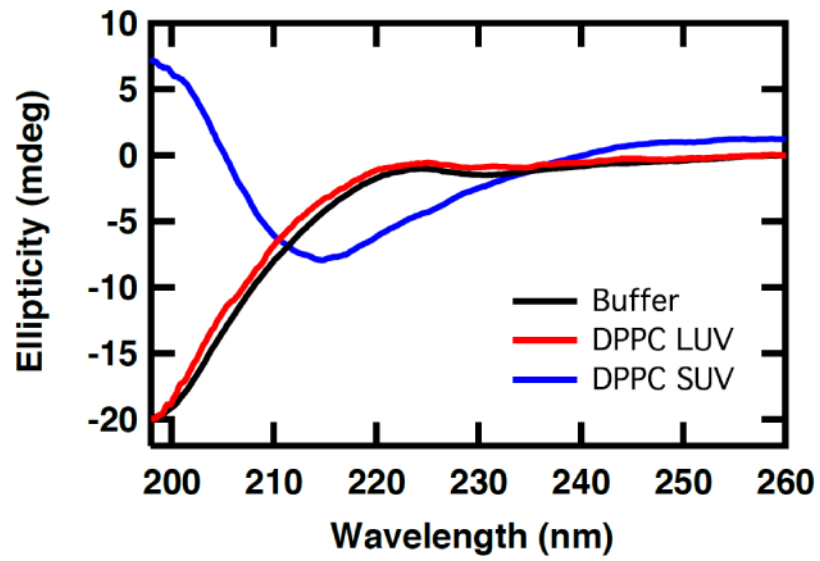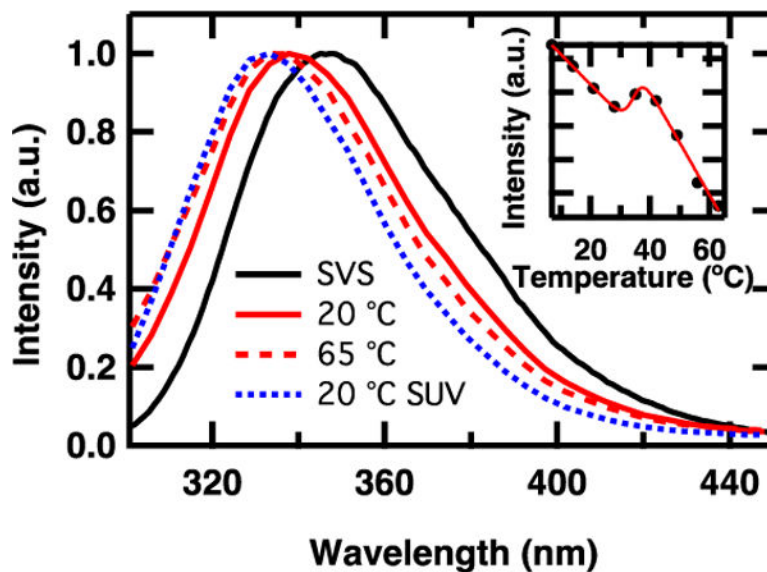
Figure 3.
Far-UV CD spectra of 60 µM SVS-V8W in 10 mM sodium phosphate buffer and 150 mM NaCl pH 7.4 (black), 2.5 mM DPPC LUV (red), and 2.5 mM DPPC SUV (blue) at 20 °C.

Figure 4.
Fluorescence spectra of 60 μM SVS-V8W in 10 mM sodium phosphate buffer and 150 mM NaCl pH 7.4 (black), 2.5 mM DPPC LUV (red), and 2.5 mM DPPC SUV (blue) at 20 °C excited at 280 nm.
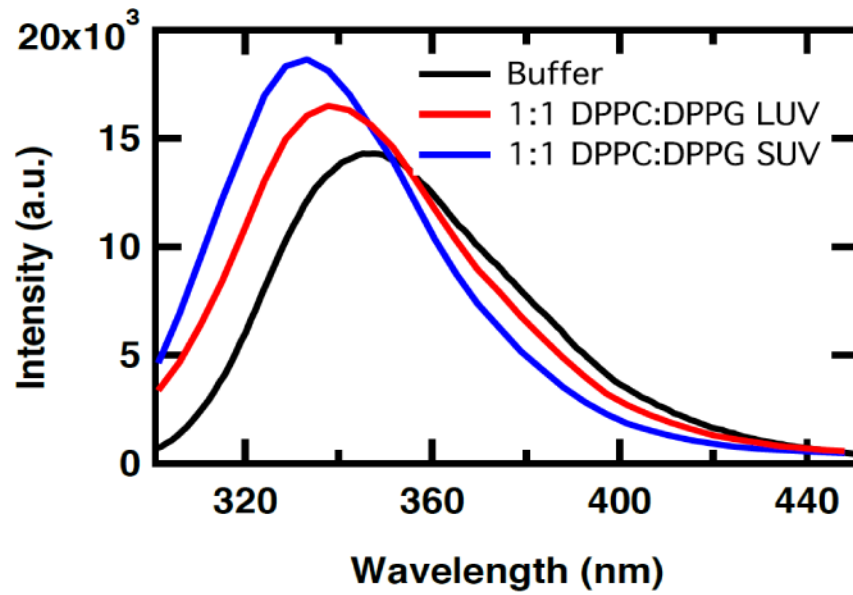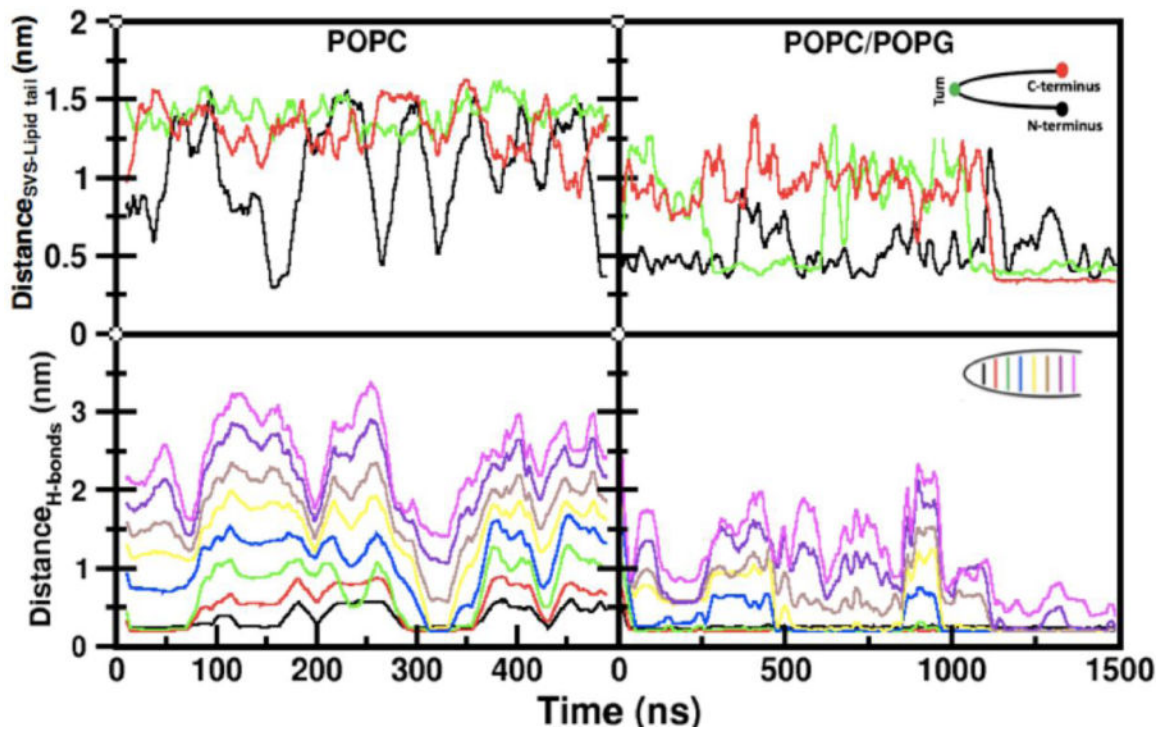
Figure 5.
Fluorescence spectra of 60 μM SVS-V8W in 10 mM sodium phosphate buffer and 150 mM NaCl pH 7.4 (black), 2.5 mM 1:1 DPPC/DPPG LUV (red), and 2.5 mM 1:1 DPPC/DPPG SUV (blue) at 20 °C excited at 280 nm.
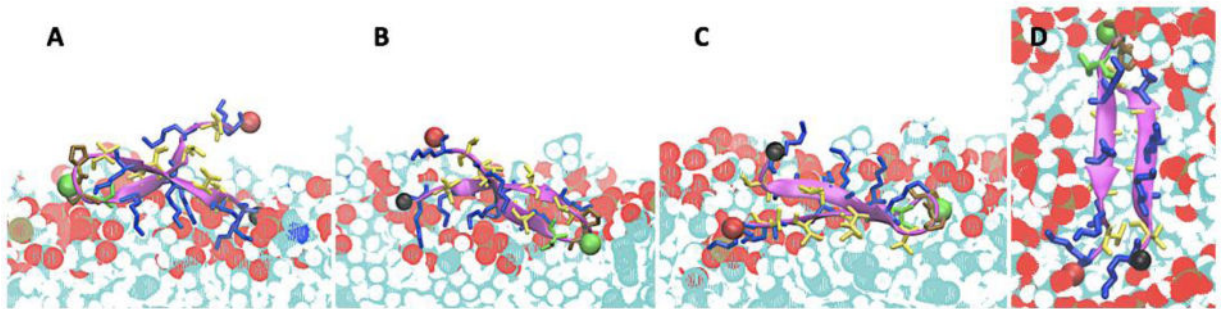
Figure 6.
Normalized fluorescence spectra of 60 μM SVS-V8W in 10 mM sodium phosphate buffer and 150 mM NaCl pH 7.4 (black), 2.5 mM 1:1 DPPC/DPPG SUV (blue dash) and 2.5 mM 1:1 DPPC/DPPG LUV (red) at 20 °C and 2.5 mM 1:1 DPPC/DPPG LUV (red dash) at 65 °C excited at 280 nm. Inset: Intensity at the wavelength maximum, 348 nm, of 60 μM SVS-V8W in 2.5 mM 1:1 DPPC/DPPG LUV acquired every 5 °C from 5 to 65 °C during the course of a temperature-dependent experiment in a 1 cm pathlength cell. The continuous line represents the best fit of the data to a sigmoid (Equation 1).
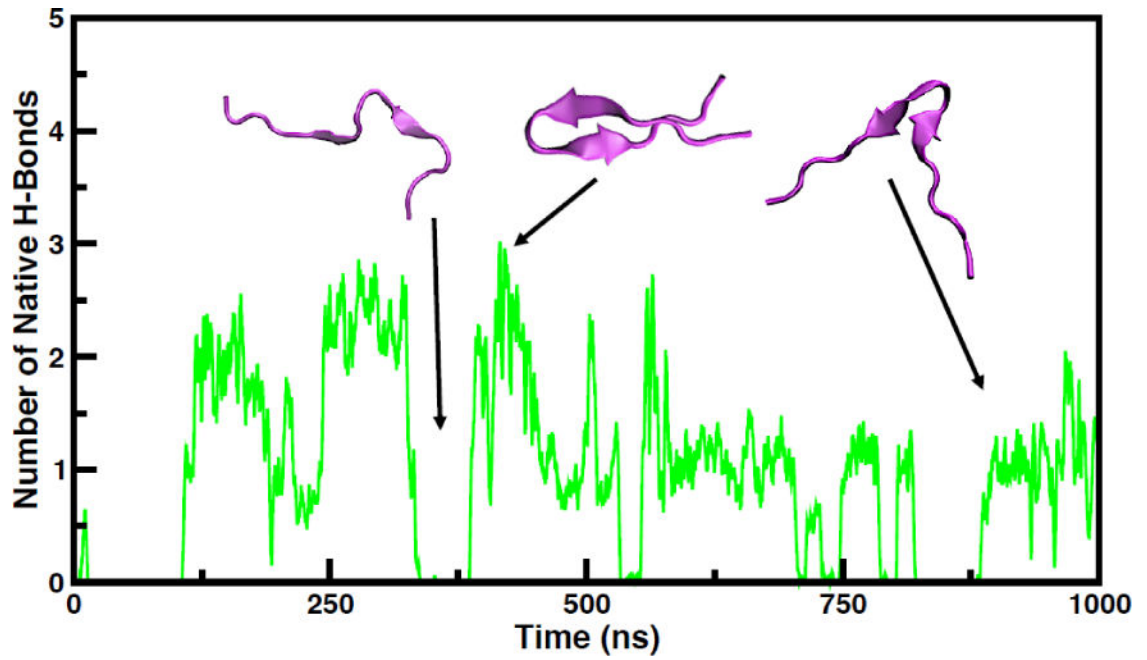
Figure 7.
Number of native hairpin SVS-1 hydrogen bonds in 1000 ns solution-phase simulation, with corresponding peptide snapshots. Folded peptides are drawn in New Cartoon method using VMD. The plot has been smoothed, showing averages over 1 ns.
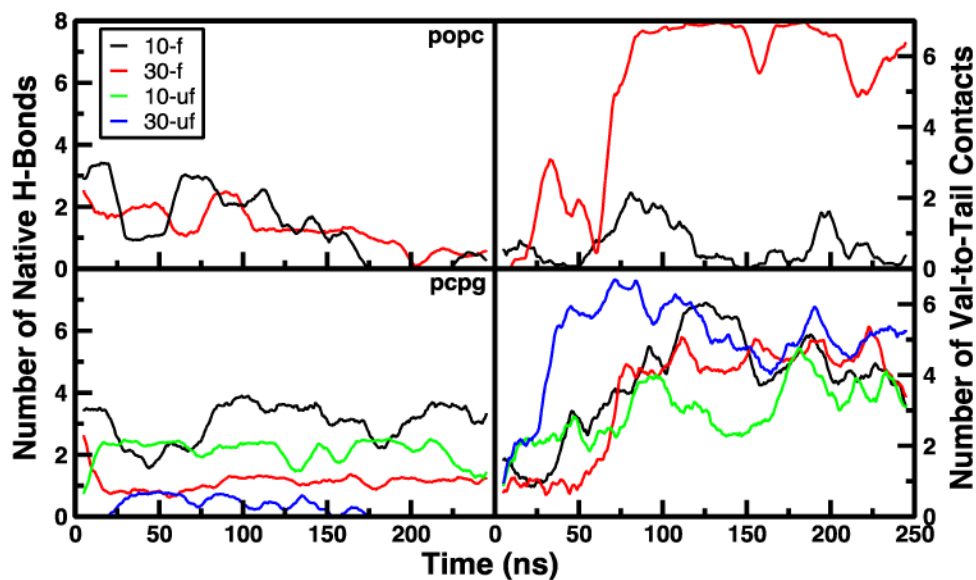
Figure 8.
Bilayer contact fluctuations and hydrogen bond formation (folding dynamics) of SVS-1 in presence of a zwitterionic POPC bilayer (500 ns) and an anionic POPC/POPG bilayer (1500 ns). Fluctuations track distances of terminal sites and center of turn to the closest acyl tail carbon. The atoms are colored based on description in Methods (See cartoon in upper right panel). Hydrogen bond order from 1-8 (starting from turn to the tail-end) are represented in order by the colors: black, red, green, blue, yellow, brown, purple and magenta (See cartoon in lower right panel). The curves represent averages smoothed over 1 ns.

Figure 9.
Snapshots from the 1500 ns simulation of SVS-1 interaction with 1:1 POPC/POPG bilayer. Figure A shows partially folded structure with strong interactions of lysine sidechains with headgroups at 1040 ns. Figure B highlights the initiation of the "flip and dip" mechanism, where the turn buries beneath the headgroups (at 1075 ns). Figure C depicts endpoint of the "flip and dip" mechanism after 50 ns (1130 ns). Figure D (top-down view) represents SVS-1 with valines inserted and lysines facing upwards into solution (end of 1500 ns simulation). Red, green, and black sites as defined in Figure 8 are shown as spheres. SVS-1 sidechains are depicted as a licorice: valine(blue), lysine(green), proline(orange) and threonine(yellow). Lipids are represented as dotted in VMD drawing method. Some lipids are removed for Figures A–C for clarity of mechanism. Water and ions removed for clarity.

Figure 10.
Number of native hydrogen bonds formed (left) and number of valine-to-tail contacts (right) for a folded or unfolded SVS-1 peptide in the presence of an anionic or zwitterionic bilayer (at 323 K) using C36m, as defined in section 2.2.4. Simulations for each of the starting configurations, folded (f) or unfolded (uf), were performed under applied surface tension factors of 10 or 30 mN/m, respectively. Curves represent averages smoothed over 1 ns.

Table 1

System components of long MD Simulations of SVS-1 in solution and presence of lipid bilayers.

Simulation	Simulation length (ns)	no. of atoms	no. of water molecules	POPC lipids	POPG lipids	SVS-1 peptides	K⁺ ions	Cl⁻ Ions
1	1000	21470	7042	0	0	1	0	9
2	500	42456	7784	140	0	1	0	9
3	1500	40470	7262	70	70	1	70	9